Sheffield Hallam University

Reactivity of a Nickel(II) Bis(amidate) Complex withmeta-Chloroperbenzoic Acid: Formation of a Potent Oxidizing Species

CORONA, Teresa, PFAFF, Florian F., ACUÑA-PARÉS, Ferran, DRAKSHARAPU, Apparao, WHITEOAK, Christopher <http://orcid.org/0000-0003-1501-5582>, MARTIN-DIACONESCU, Vlad, LLORET-FILLOL, Julio, BROWNE, Wesley R., RAY, Kallol and COMPANY, Anna

Citation:

Copyright and re-use policy

Reactivity of a nickel(II) bis-amide complex with H*m*CPBA: formation of a potent oxidizing species

Teresa Corona,[a] Florian Pfaff,[b] Ferran Acuña-Parés,[a] Apparao Draksharapu,[c] Christopher J. Whiteoak,[a] Vlad Martin-Diaconescu,[a] Julio Lloret-Fillol,[a,d] Wesley R. Browne,[c] Kallol Ray,[b] Anna Company*[a]

[a] T. Corona, F. Acuña-Parés, Dr. C. J. Whiteoak, Dr. V. Martin-Diaconescu, Dr. J. Lloret-Fillol, Dr. A. Company Grup de Química Bioinorgànica, Supramolecular i Catàlisi (QBIS-CAT), Institut de Química Computacional i Catàlisi (IQCC), Departament de Química, Universitat de Girona, Campus Montilivi, E17071 Girona (Catalonia - Spain). Phone: +34 972 41 98 42. Fax: +34 972 41 81 50. E-mail: anna.company@udg.edu [b] F. Pfaff, Dr. K. Ray Humboldt Universität zu Berlin, Department of Chemistry, Brook-Taylor Strasse 2, 12489 Berlin (Germany) [c] Dr. A. Draksharapu, Dr. W. R. Browne Stratingh Institute for Chemistry, Faculty of Mathematics and Natural Sciences, University of Groningen, Nijenborgh 4, 9747 AG Groningen, The Netherlands [d] The current address of J. Lloret-Fillol is: Institute of Chemical Research of Catalonia (ICIQ), Av. Països Catalans 16, 43007 Tarragona, Spain

Abstract: Herein we report the formation of a highly reactive nickel-oxygen species that has been trapped following reaction of a nickel(II) precursor (bearing a macrocyclic bis-amidate ligand) with *meta*-chloroperbenzoic acid. This compound is only detectable at temperatures below 250 K and it is much more reactive towards organic substrates (C-H bonds, C-C double bonds and sulfides) than the previously reported well-defined Ni-oxygen species. Remarkably, this species is formed by heterolytic O-O bond cleavage of a Ni-H*m*CPBA precursor as supported by experimental and computational methods. On the basis of spectroscopic and DFT calculations this reactive species is proposed to be a Ni^{III}-oxyl compound.

Introduction

The study of high-valent nickel complexes in particular and the redox chemistry of nickel in general has attracted the attention of the bioinorganic chemistry community to provide models of nickel-containing enzymes that catalyze redox processes.[1] Enzymes with redox-active nickel sites include [NiFe]-hydrogenases,[2] CO dehydrogenase,[3] acetyl-CoA synthase[4] and Ni superoxide dismutase.[5] Moreover, high-valent nickel species have been frequently postulated as key reaction intermediates both in the catalytic cycle of oxidation reactions[6, 7] and in coupling reactions.[8, 9]

In the field of oxidation chemistry, nickel-oxygen species are perceived to be formed upon homolytic or heterolytic O-O bond cleavage of the oxidant bound to a Ni^{II} precursor. For example, alkane oxidation catalyzed by [Ni^{II}(tpa)(OAc)(H$_2$O)]$^+$ (tpa = tris(pyridylmethyl)amine) and related systems using the oxidant H*m*CPBA (*meta*-chloroperbenzoic acid) occur through a Ni^{III}-oxo or Ni^{II}-oxyl intermediate species.[10-12] Furthermore, experimental and theoretical studies have indicated that a [Ni^{III}-O]$^+$ species is a potent oxidant in the gas phase for the conversion of methane to methanol.[13, 14] Evidences for Ni^{IV}-oxygen intermediates are, in contrast, limited.[7]

In contrast to the large number of mononuclear Mn- and Fe-oxygen species reported in the literature over the past decade,[15] relatively few examples of such species based on late transition metals such as nickel have been described. Recently, Ray and co-workers have shown that a nickel(II)-acylperoxo coordinated to TMG$_3$tren (TMG$_3$tren = tris[2-(*N*-tetramethylguanidyl)ethyl]amine) is the precursor to a nickel(III)-oxo/hydroxo compound that is able to perform oxo-transfer and C-H activation with a rate-determining H-atom abstraction.[16] Moreover, Hikichi and co-workers reported the selective hydroxylation of cyclohexane catalyzed by tris(pyrazolyl)borate-based nickel(II) complexes with H*m*CPBA.[17] For the latter systems thermally stable nickel(II)-acylperoxo species, were detected spectroscopically and characterised crystallographically.[17] Evidence for the formation of a transient [Ni^{IV}(OH)(cyclam)]$^{2+}$ competent to epoxidase olefins was gathered for the reaction of the corresponding nickel(II) precursor with H$_2$O$_2$ in acidic media.[7] Most recently, McDonald and co-workers reported the characterization and reactivity of a terminal nickel(III)-oxygen adduct which was able to perform hydrogen-atom abstraction of weak C-H bonds and oxygen-atom transfer to triphenylphosphine.[18]

Literature precedents show that pincer-like tridentate 2,6-pyridinecarboxamidate ligands can support well-defined nickel(III) or nickel(IV) complexes[19] (including a Ni^{III}-OCOOH species[18]) and a highly reactive Cu^{III}-OH motif, as reported by Tolman and co-workers.[20] Here, we show that reaction of [Ni^{II}(L)] (**1**) (where L is a tetradentate dianionic macrocyclic ligand combining two amidates, one pyridine and one aliphatic amine, Figure 1a) with H*m*CPBA forms a transient nickel-oxygen species (**2**) that has been characterised spectroscopically. Compound **2** is only stable at sub-ambient temperatures (< 240 K) and it is more reactive towards organic substrates (C-H bonds, C-C double bonds and sulfides) than the previously reported well-defined Ni-oxygen species. Experimental and computational methods indicate that, remarkably, this species is formed by heterolytic O-O bond cleavage.

Results and Discussion

The ligand H$_2$L was synthesized following a 4-step synthetic route (Scheme S1). Selective methylation of the central amine of commercially available *N*-(2-aminoethyl)-1,3-propanediamine required prior protection of the two terminal amines with phthalic

anhydride. After methylation and amine deprotection with hydrazine, 1+1 cyclization with 2,6-pyridinedicarbonyl chloride yields H_2L. This step was the most critical due to formation of 2+2 macrocyclic by-products. Thus, the reaction was carried out under conditions of high dilution in order to obtain the desired 1+1 product in at least modest yields (see Supporting Information). Reaction of equimolar amounts of H_2L and $[Ni^{II}(CF_3SO_3)_2(CH_3CN)_3]$ with 2 equiv NaH under anaerobic conditions in acetonitrile afforded the complex $[Ni^{II}(L)]$ which co-crystallizes with $NaCF_3SO_3$ (**1**·$NaCF_3SO_3$) in 72% yield. The nickel center is present in a square planar geometry with coordination to the pyridine, an aliphatic tertiary amine and two amidate units *trans* to each other (Figure 1b). The bond lengths Ni-N_{py} (1.796 Å), Ni-N_{CH3} (1.929 Å) and Ni-N_{amide} (1.85-1.87 Å) are consistent with those of previously reported Ni^{II} square planar complexes with pyridine, amine or amidate-based ligands.[21-23] The geometry renders the complex diamagnetic enabling characterisation by 1-D, 2-D, ^{1}H-NMR and ^{13}C-NMR spectroscopy (Figure S1-S4). As expected, the complex does not present C_2 symmetry and the β protons of the pyridine ring appear as two well-resolved doublets at 7.43 and 7.36 ppm. High resolution QTOF-MS showed a major peak at m/z 341.053 with an isotopic pattern fully consistent with $[Ni(L)]+Na^+$.
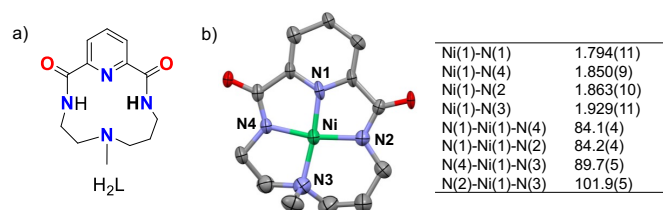

Ni(1)-N(1)	1.794(11)
Ni(1)-N(4)	1.850(9)
Ni(1)-N(2	1.863(10)
Ni(1)-N(3)	1.929(11)
N(1)-Ni(1)-N(4)	84.1(4)
N(1)-Ni(1)-N(2)	84.2(4)
N(4)-Ni(1)-N(3)	89.7(5)
N(2)-Ni(1)-N(3)	101.9(5)

Figure 1. a) Schematic representation of H_2L. b) X-ray structure and selected bond lengths (Å) and angles (°) for **1**·$NaCF_3SO_3$. Hydrogen atoms and co-crystallized $NaCF_3SO_3$ have been omitted for clarity.

Monitoring the reaction of **1** with 3 equiv H*m*CPBA in acetonitrile at -30 ºC by UV/vis absorption spectroscopy indicated the formation of a metastable dark yellow species (**2**) with an absorption band at 420 nm (ε > 7000 $M^{-1}cm^{-1}$) and a shoulder at 580 nm (ε > 800 $M^{-1}cm^{-1}$). The half-life of this species at -30 ºC was 4.5 h. Compound **2** was not detected when the reaction was carried out at room temperature.
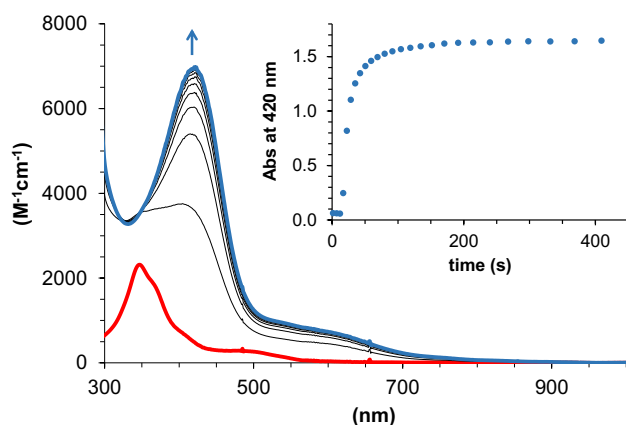

Figure 2. UV/vis absorption spectral changes observed upon reaction of **1** with 3 equiv H*m*CPBA in CH_3CN at -30 ºC to form **2**. Inset: kinetic trace at 420 nm.

Species **2** reacts with various substrate classes. Indeed, the decay of **2** was accelerated substantially by the addition of thioanisole as ascertained by UV/vis absorption spectroscopy (Figure S5). Under conditions of excess substrate the decay in absorbance showed pseudo-first order behaviour and could be fitted with a monoexponential function. The value of k_{obs} varied linearly with thioanisole concentration, affording a second order rate constant (k) of 0.56 $M^{-1}s^{-1}$ at -30 ºC (Figure S6). Reaction rates were dependent on the substituent at the *para* positon of the sulfide. The logarithm of the second order rate constants of a series of *para*-substituted methyl phenyl sulfides, *p*-X-thioanisoles (k_X, X = Me, Cl, CN) showed correlation with the Hammett parameter (σ$_p$) with a reaction constant (ρ) of -0.86 (Figure 3a). The negative ρ value indicates build-up of positive charge at the transition state and hence **2** has an electrophilic character in these reactions. Moreover, a plot of the log(k_x) against the one-electron oxidation potentials of each *p*-X-thioanisole ($E°_{ox}$) afforded a linear correlation with a slope of -1.84 (Figure S7), which indicates that the oxidation of sulfides by **2** occurs via a direct oxygen-atom transfer rather than electron-transfer oxidation.[24]
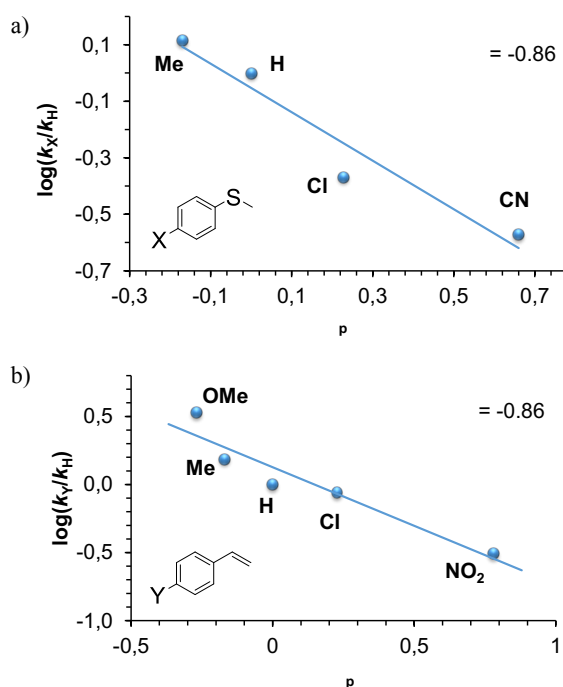

Figure 3. Hammett plot, log(k_X/k_H) vs the Hammett parameter (σ$_p$), for the reaction of **2** in acetonitrile at -30 ºC with (a) *p*-X-thioanisoles and (b) *p*-Y-styrenes.

Compound **2** also behaves as an electrophilic O-atom transfer reagent towards alkenes. Thus, under pseudo-first order reaction conditions, a second order rate constant (k) of 0.18 $M^{-1}s^{-1}$ was obtained for the oxidation of cyclooctene, while this value decreased to 0.04 $M^{-1}s^{-1}$ for 1-octene. Reaction of **2** with a series of *para*-substituted styrenes, *p*-Y-styrenes (Y = OMe, Me, H, Cl and NO$_2$), further evidences the electrophilic character of **2** affording a negative reaction constant (ρ) of -0.86 (Figure 3b). Analysis of the final oxidation products for the reaction of **2** with alkenes at -30 ºC indicates the formation of the corresponding epoxides with yields (with respect to the nickel complex) ranging from 140% for cyclooctene oxide and styrene oxide to 50% for 1,2-epoxyoctane. Despite the fact that peracids are well-known to

be capable of directly oxidizing alkenes without the mediation of a metal complex,[25] control experiments (in the absence of nickel complex) indicate that no epoxide was formed by direct reaction of HmCPBA with the alkene substrate under the current reaction conditions (reaction mixture was quenched with excess NaHSO$_3$ after full decay of **2** at -30 ºC). These results suggest that the slight excess of oxidant necessary to maximize the formation of **2** triggered a catalytic reaction as a background, which explains the yields over 100% obtained for some of the substrates tested. Thus, the combination of **1** and HmCPBA might afford an efficient catalytic system for the oxidation of selected substrates (see below).

Compound **2** could perform hydrogen-atom abstraction from O-H bonds reacting with 2,4,6-tri-*tert*-butylphenol to quantitatively form the corresponding phenoxyl radical, manifested in the appearance of an intense absorption band at 626 nm characteristic of this radical.[26] Remarkably, **2** was also reactive towards hydrocarbon substrates with activated methylene C-H bonds, such as fluorene, 1,4-cyclohexadiene, 9,10-dihdyroanthracene and xanthene, again obeying pseudo-first order kinetics under conditions of excess substrate with k_{obs} values linearly dependent on substrate concentration (Figure S11). The obtained second-order rate constants were adjusted for the reaction stoichiometry to yield the corrected rate constants (k'). As expected the rate constants decreased with the increase of C-H bond dissociation energy (BDE). More interestingly, log(k') values correlated linearly with BDE with a slope of -0.23. Such a linear relationship between reaction rates and BDE provides strong evidence for hydrogen-atom abstraction as the rate-determining step for the oxidation. Parallel reactions with deuterated 9,10-dihydroanthracene (d_4-DHA) yielded a kinetic isotope effect (KIE) of 4 (Figure S12), a value consistent with a C-H bond cleavage being the rate-determining step.[27, 28]
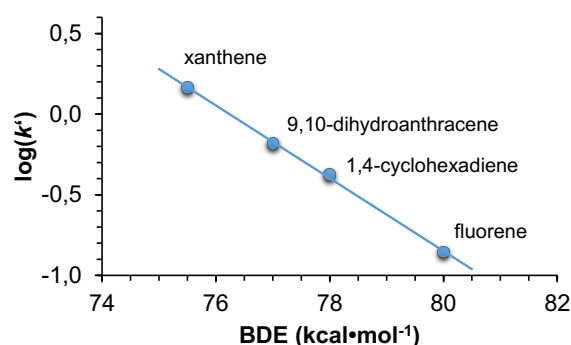

Figure 4. Plot of log(k') (determined at -30 ºC) against the C-H BDE for the oxidation of alkanes with activated C-H bonds by **2**.

Reaction of **2** with substrates bearing stronger C-H bonds was also examined. Addition of alkanes such as toluene, ethylbenzene or cyclohexane (300 equiv) to a solution of **2** at -30 ºC caused the decay of its characteristic band at 420 nm with significantly higher rates than in the absence of these substrates (Figure S13). However, decay of **2** did not follow simple single-exponential functions, most probably because the background catalytic reaction significantly interferes with the kinetic trace. Analysis of the final organic products showed the formation of oxidized products (benzaldehyde, acetophenone or cyclohexanone, respectively) in yields ranging from 21 to 50% yield with respect to **1**.

The oxidation power of **2** was compared with that of previously spectroscopically characterized nickel(II)-acylperoxo complex [Ni^{II}(Tp^{CF3Me})(mCPBA)][29] and nickel(III)-hydroxo(oxo) compound [Ni^{III}(O(H))(TMG$_3$tren)]$^{n+}$[16] obtained by reaction of their Ni^{II} precursors with HmCPBA (Table 1). Interestingly, **2** reacts more than 200 times faster with C-H bonds than [Ni^{III}(O(H))(TMG$_3$tren)]$^{n+}$ at the same temperature (-30 ºC). The same reaction is up to 3-orders of magnitude faster compared to [Ni^{II}(Tp^{CF3Me})(mCPBA)], while reaction towards *p*-Y-styrenes occurs about 50 times faster. However, the much higher temperature (+70 ºC) used for the reactivity studies with the Tp-based system indicates that differences with respect to **2** are, indeed, much greater. Overall, compound **2** is significantly more active than previously reported well defined Ni/mCPBA species. Comparison with the reactivity of the nickel(III)-oxygen species adduct recently reported by McDonald and co-workers[18] is hampered because studies with this compound are limited to compounds containing weaker O-H bonds (2,6-di-*tert*-butylphenol) and C-H bonds (1-benzyl-1,4-dihydronicotinamide, BDE = 64 kcal•mol^{-1}) or triphenylphosphine.

Table 1. Second-order rate constants (k) for the oxidation of different substrates by **2**, [Ni^{III}(O(H))(TMG$_3$tren)]$^{n+}$ and [Ni^{II}(Tp^{CF3Me})(mCPBA)].

k, M^{-1}s^{-1}	compound 2 (-30ºC)	[Ni^{III}(O(H)) (TMG$_3$tren)]$^{n+}$ (-30ºC)[16]	[Ni^{III}(Tp^{CF3Me}) (mCPBA)] (+70ºC)[29]
xanthene	2.93	0.0131	0.0018
9,10-dihydroanthracene	2.62	0.0125	0.00051
1,4-cyclohexadiene	1.69	0.0073	0.019
fluorene	0.28	-	0.0010
styrene	0.45	-	0.0088
4-methylstyrene	0.69	-	0.017
4-methoxystyrene	1.51	-	0.022

TMG$_3$tren = tris[2-(*N*-tetramethylguanidyl)ethyl]amine
Tp^{CF3Me} = hydrotris(3-trifluoromethyl-5-methylpyrazolyl)borate

Given the high reactivity of compound **2** towards several substrate classes including alkanes bearing strong C-H bonds, we tested the ability of the **1** to act as catalyst in the oxidation of cyclohexane using HmCPBA as oxidant. Slow addition of HmCPBA (150 equiv) to a solution containing **1** and cyclohexane (15000 equiv) afforded a mixture of cyclohexanol (A) and cyclohexanone (K) with a total turnover number of 100 and A/K ratio of around 1, with an overall 67% yield with based on oxidant. Blank experiments in the absence of the nickel catalyst showed the formation of only trace amounts of oxidized products (<0.5% yield).

Further insight into the nature of the oxidizing species was gained through the oxidation of *cis*-1,2-dimethylcyclohexane and adamantane. Oxidation of *cis*-1,2-dimethylcyclohexane (150 equiv) by **1** (1 equiv) using HmCPBA (150 equiv) as oxidant afforded the corresponding tertiary alcohol product with 84% retention of configuration (RC) of the tertiary carbons. Under similar experimental conditions, adamantane was oxidized with a high preference for the tertiary carbon with a 3º/2º ratio of 18 (corrected according to the number of equivalent secondary and tertiary C-H bonds). Much lower RC and 3º/2º ratios would be obtained if freely diffusing radicals, hydroxyl or alkxoyl, were involved.[30] These data indicate that a metal-based oxidant, most

likely the spectroscopically detected species **2** (vide infra), is mainly responsible for the observed oxidation reactions.
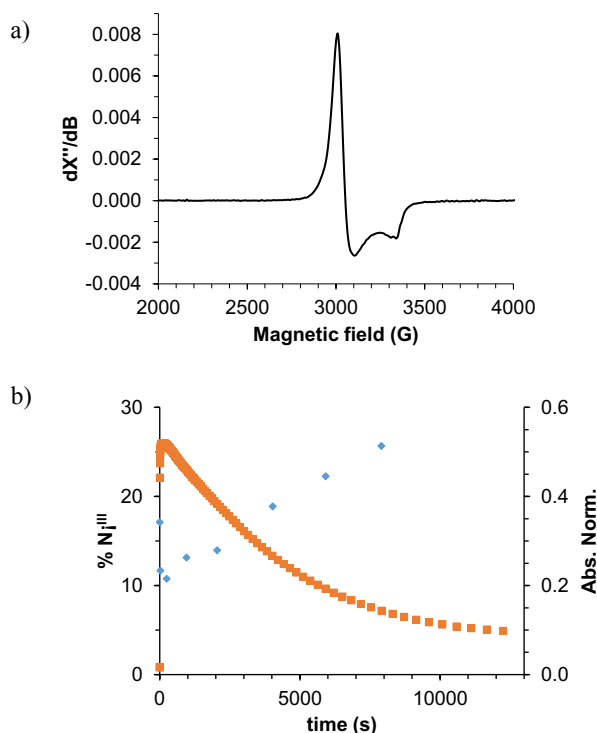

Figure 5. a) EPR spectrum of the reaction of **1** (1.9 mM) with 3 equiv of H*m*CPBA in acetonitrile at -30 ºC after 60 s under Ar. b) Orange dots correspond to time-course of the self-decay of **2** generated by adding 3 equiv H*m*CPBA to **1** (0.5 mM) in CH$_3$CN at -25 ºC followed by UV/vis absorption spectroscopy (λ = 580 nm). Blue dots correspond to the intensity of the EPR signal at gx = 2.27, gy = 2.20 and gz = 2.03 corresponding to nickel(III).

Characterization of **2** by cryospray ionization mass spectrometry (CSI-MS) at -30 ºC revealed a clean spectrum with a major peak at m/z 318.06, with an isotopic pattern fully consistent with [Ni^{III}(L)]$^+$. Interestingly, CSI-MS monitoring of the reaction of **2** with 1-octene showed the progressive formation of nickel(II) species (m/z = 355.03). Instead, for 9,10-dihydroanthracene no nickel(II) was formed along the reaction and only nickel(III) was observed (m/z = 318.06) (Figures SX-SX). In any case, in the presence or absence of substrate the MS spectrum of the reaction mixture obtained upon warming up at room temperature only exhibited signals corresponding to nickel(II) species with oxidized/dehydrogenated ligand (m/z = 355.03).

EPR spectra of samples taken over the course of the decay of **2** indicated the presence of a nickel(III) species with *g* values of g_x = 2.27, g_y = 2.20 and g_z = 2.03 corresponding to S = 1/2 (Figure 5a).[31-34] However, the time-dependence of the change in the intensity of the EPR signal did not directly correlate with that of the UV-vis absorbance at 420 nm (or its shoulder at 580 nm) assigned to **2**. The concentration of nickel(III) steadily increased over time even after disappearance of the chromophore (Figure 5b). These data indicate that the signal of the nickel(III) corresponds to a decayed species of **2** which is not responsible for the observed oxidation chemistry. Interestingly, the EPR signal related to nickel(III) completely disappeared when the sample was warmed to room temperature, highlighting the thermal instability of this species.

To help further characterize the Ni center of **2**, XAS was applied at the metal K-edge. The pre-edge of **2**, associated with 1s → 3d transitions, occurs at ~ 8333.5 eV and has a normalized area of 0.16, indicating the presence of a high valence Ni species (Supplementary Figure S3). Generally for Ni^{II} complexes the 1s → 3d transitions occur around ~ 8332 eV and are 2 to 3 fold less intense.[35] A higher oxidation state for **2** is further emphasized by a higher rising edge energy determined using the half-height method. In **2** this energy is at ~ 8343.4 eV, which is ~1.5 - 2 eV higher in energy than those reported for Ni^{II}[35] consistent with a Ni^{III} species.[36-38] Previous studies on Ni-oxido and Ni-cyclam derivatives show a 1.5 to 2 eV shift going from Ni^{II} to Ni^{III}, while a ~4 eV shift would be expected for Ni^{IV}.[36-38] When compared to Ni foil this translates to a ~ 4 eV shift for Ni^{III}, while Ni^{IV} would be expected to have a ~6 eV shift to higher energy (Supplementary Figure S3).[37] Therefore the XANES spectra of **2** is most consistent with a Ni^{III} oxidation of the metal center. The Fourier transformed EXAFS spectra of **2** is shown in Figure X1. Three scattering shells are implied by the features at 1.4, 1.8 and 2.2 Å. Single scatter fits are consistent with the first two peaks corresponding to two N/O scattering shells (Supplementary Table S1). On the other hand, the feature at 2.2 Å is consistent with contributions from multiple scattering of the pyridine ring. Several multiple scattering models were attempted (see Supplementary Table S2) and the EXAFS analysis converged on a model with two longer metal - N/O bonds at ~ 2.12 Å, and three shorter N/O bonds at ~ 1.88 Å including the pyridine ligand (Table X1).

Table X1: EXAFS multiple scattering model showing Ni-ligand bond distances and coordination number for complex 2; (E$_0$ fixed to 8344.2 eV and S$_0$ set to 0.9).

model	path	Δr (Å)	σ^2 (x10^3 Å^2)	%R	χ^2_v
N$_2$N$_3$(Pyr)	2 N$^{2.0}$	0.12(1)	1.9(6)		
	3 N$^{1.8}$	0.08(1)	1.9(6)	8.7	7.2
	1 Pyr*	0.08(1)	6(2)		

*refers to the pyridine scattering paths not including the primary N-Ni single scatter path
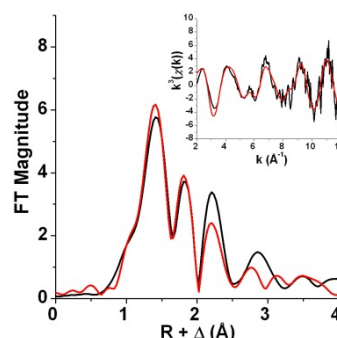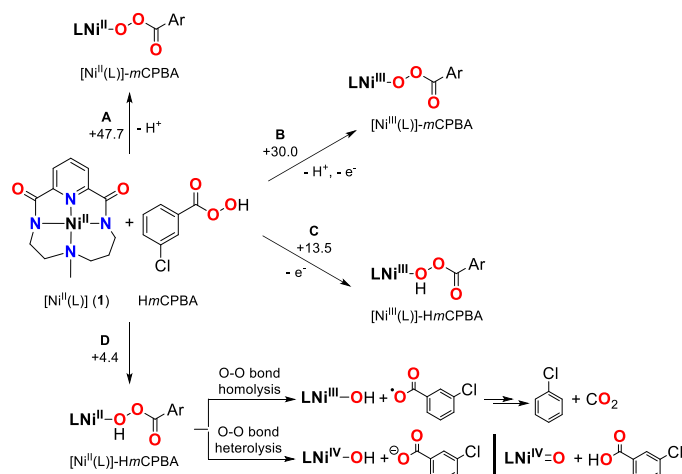

Figure X. Fourier-transformed EXAFS spectra of **2** (no phase correction, FT window 2 - 12 Å^{-1}): *black line* data, *red line* best fit. Inset: k^3-weighted unfiltered EXAFS spectra: *black line* data, *red line* best fit.

Scheme 1. Possible pathways (A-D) studied by DFT corresponding to the reaction of **1** with H*m*CPBA in acetonitrile. Free energies are in kcal•mol^{-1} at -30 °C.

DFT calculations were carried out to explore the possible nature of **2**. Literature precedents indicated four distinct mechanistic scenarios for the reaction of **1** with H*m*CPBA (reactions A-D, Scheme 1). Pathway A involves the formation of a Ni^{II}-acylperoxy species, [(L)Ni^{II}-*m*CPBA]$^{-}$. However, this process was considered kinetically and thermodynamically unfeasible due to the high free energy difference of [(L)Ni^{II}-*m*CPBA]$^{-}$ relative to the starting reactants (ΔG^o = +47.7 kcal•mol^{-1}). This difference may be rationalized by the acidity of H*m*CPBA (pK$_a$ = 31) which was computed to be much lower than that of **1-H$^+$** (pK$_a$ = 7) in acetonitrile, so that proton transfer from H*m*CPBA to **1** is unfavourable. An alternative mechanism involves the formal oxidation of Ni^{II} to Ni^{III} (accompanied by the 1e$^-$ reduction of H*m*CPBA to give the radical anion), and the subsequent coordination of another H*m*CPBA or *m*CPBA molecule to the +3 metal centre. However, DFT calculations suggest the thermodynamic unviability of these two processes (pathway B: ΔG^o = +30.0 kcal•mol^{-1}; pathway C: ΔG^o = +13.5 kcal•mol^{-1}) centre. This result is in agreement with the EPR data, which indicated that regarded the Ni(III) species is not related to the chromophore **2**.

Instead, the complexation of **1** with H*m*CPBA is thermodynamically reasonable with a ΔG^o value of +4.4 kcal•mol^{-1} (pathway D, Scheme 1). [(L)Ni^{II}]-H*m*CPBA may evolve through two different reaction pathways as previously postulated for other nickel systems (Scheme 1): a) homolytic O-O bond cleavage to form Ni^{III}-hydroxo species together with a carboxyl radical, which decomposes to give chlorobenzene and carbon dioxide; or b) heterolytic O-O bond cleavage to form a Ni^{IV}-oxo intermediate and the corresponding benzoic acid. Computational studies indicate that the homolytic pathway is kinetically unfavorble by +30.0 kcal•mol^{-1} (Scheme 2). Instead, the O-O heterolysis shows a lower barrier of only +9.0 kcal•mol^{-1} to afford a Ni-oxygen species. Interestingly, chromatographic analysis of the reaction mixture after self-decay of **2** did not show the presence of chlorobenzene or CO$_2$ but instead the formation of quantitative amounts of *meta*-chlorobenzoic acid (H*m*CBA) was ascertained by NMR and GC-MS, indicating that an O-O heterolysis pathway is following under the experimental conditions (Figure S16). Finally, addition of **1** to preformed **2** causes the immediate decay of the latter species as followed by UV/vis absorption spectroscopy (Figure S18). The ESI-MS at room temperature of the reaction mixture showed the

presence of Ni^{III} suggesting that comproportionation was occurring between **2** (formally Ni^{IV}) and **1** (Ni^{II}) to give Ni^{III}(L)$^+$ (m/z = 318.0617) (Figure S17). Thus, both experimental and theoretical data point towards an O-O heterolytic pathway as the most plausible mechanism. Moreover, according to DFT calculations, the terminal oxygen atom bears an interaction with the acidic proton of the acid by-product (H*m*CBA). This compound would carry out the oxidation of the substrate.

Formally **2** is assigned formally as a nickel(IV)-oxo compound. However, analysis of the Hirshfeld's spin density on the nickel center (ρ(Ni) = 0.66) and the oxo moiety (ρ(O) = 1.29) suggests that it is best described as a Ni^{III}-O$^{\bullet}$ species (Tables S4 and S5, Figure S19). Interestingly, inspection of the spin natural orbitals (SNOs) of complex **2** shows two single occupied orbitals: a $\sigma^*(d_z^2/p_z)$ distributed between the Ni and O centres and a p$_y$ orbital centered on the terminal oxygen (Figure S20). This electron distribution may be the responsible for the weakening of the Ni-O bond (1.950 Å) and the significant oxyl character of the oxygen group. Moreover, the Mayer index for the Ni-O bond is about 0.6, in agreement with the half broken σ bond and the lack of π bonding showed in the SNOs. Finally, to better understand the nature of the Ni-O bond, an AIM analysis was performed on **2**. We found negative but close to zero values of $\nabla^2 \rho$ (r) and H(r), which suggests a very weak Ni-O interaction with almost no covalent character (Figure S20). Therefore, the DFT analysis of the electronic structure of [Ni^{III}(L)(O$^{\bullet}$)] reveals that Ni and O atoms are weakly connected, making the terminal oxygen highly reactive.

The experimental EXAFS distances are consistent with the Ni^{III}-oxyl radical theoretical model having three shorter and two longer N/O bonds. The Ni^{III}-oxyl radical model predicts a pyridine-Ni bond of 1.85 Å, with the two proximal Ni-N bonds at 1.86 and 1.90 Å, consistent with the 1.88 Å N/O scattering shell. The Ni^{III}-oxyl radical model also predicts two longer bonds for Ni-O (1.95 Å) and Ni-N (1.96 Å), corresponding to the two longer N/O distances at 2.12 Å derived from EXAFS. This is well within the resolution of the EXAFS single scatter fits (~ 0.14 Å) for the long Ni-N/O distances.

Resonance Raman of **2** in frozen acetonitrile (77 K) showed enhancement of two sets of bands at 450 and 477 cm^{-1} and 736 and 879 cm^{-1}, which decrease in intensity concomitant with the disappearance of the absorbance of **2** (Figure 6). Simulation of the Raman spectra of [Ni^{III}(L)(O$\bullet$)]-H*m*CBA using DFT methods predicted a Ni-O vibration at 433 cm^{-1} and a ligand-based stretching vibration at 443 cm^{-1} (Figure S22). Thus, within error, experimental and theoretical results are in agreement for the first set of bands at 450 and 477 cm^{-1}. However, the other sets of bands at 736 and 879 cm^{-1} are tentatively assigned to Ni-O and O-O stretching modes, respectively, in [(L)Ni^{II}(HOOCOAr)]$^{2+}$ species.
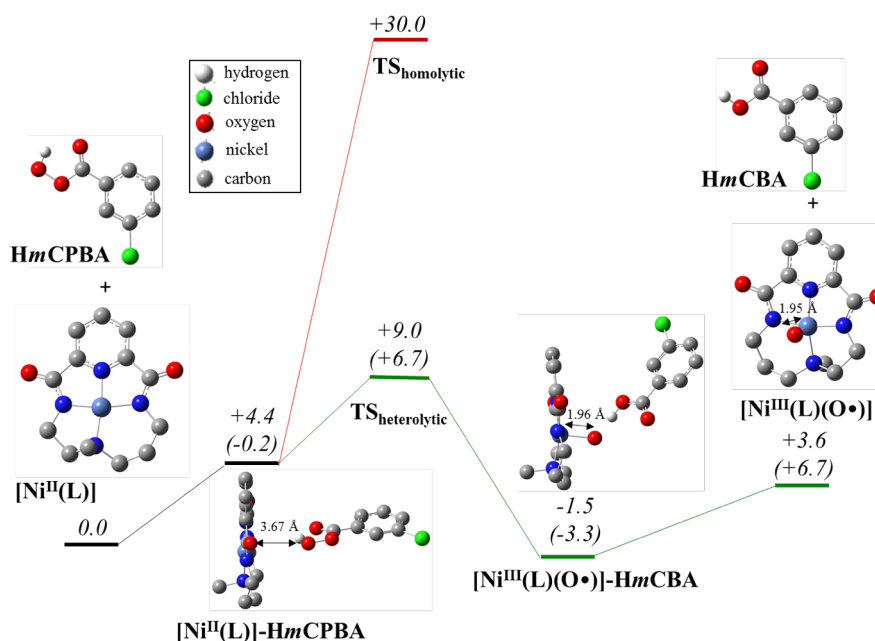
Scheme 2. Energetic profile of pathway D for the reaction of **1** with H*m*CPBA in CH₃CN (homolytic and heterolytic O-O bond cleavage). Free energies in kcal•mol⁻¹ at -30 ºC. ΔE$_{ZPE}$ in kcal•mol⁻¹ are shown in parentheses.
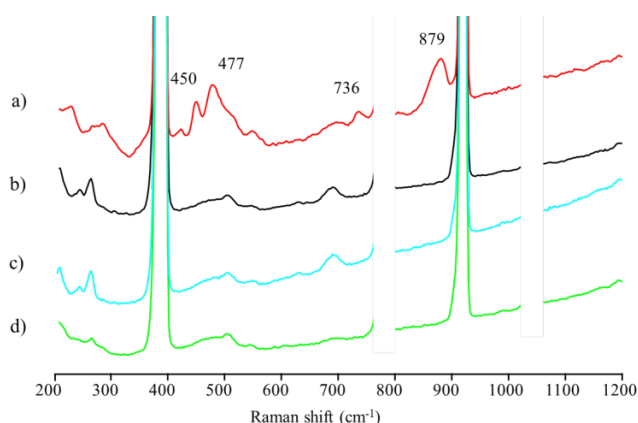

Figure 6. Resonance Raman spectra (λ$_{exc}$ 457 nm) in frozen acetonitrile (77 K) of: a) compound **2** formed after reaction of **1** (0.24 mM) with 3 equiv H*m*CPBA at -30ºC; b) H*m*CPBA (0.72 mM); c) Compound **1** (0.25 mM); d) Decomposed compound **2**.

Formulation of **2** as a nickel(III)-oxyl species is consistent with the DFT calculations and with the fact that a heterolytic O-O bond cleavage is experimentally observed (formation of H*m*CBA as reaction by-product). This formulation would also be in agreement with the EPR and NMR silence of **2** and with the EXAFS data. In CSI-MS, the lack of signal with intensity time-profiles similar to those observed by UV/vis absorption spectroscopy agrees with the neutral character of compound **2**. Finally, reaction of **2** with 1-octene (100 equiv) in CH₃CN at -30 ºC in the presence of ¹⁸O-labeled water affords the corresponding epoxide product 7% ¹⁸O-labeled. These data indicate that water exchange can occurs prior to reaction with substrates, as previously observed for other metal-oxo species.[39]

The formulation of **2** as a nickel(III)-oxyl species is controversial. Up to date, metal-oxyl species have been postulated several times but they have been scarcely directly detected.[40, 41] A possible alternative to this mechanism that would also agree with all the experimental observations would be the formulation of **2** as the [(L)Ni^II-H*m*CPBA] adduct, a precursor of the high-valent nickel species (Scheme 3). However, this would not agree with XAS data that supports a metal center with a higher valence. Moreover, reaction of **1** with an aliphatic peracid such as pernonanoic acid under the same conditions as those used for the generation of **2** (3 equiv peracid, CH₃CN, -30 ºC) affords a UV/vis absorption spectrum almost identical to that of **2** with a characteristic absorption band centred at 416 nm (Figure SX). Given the different nature of the two peracids (pernonanoic acid and H*m*CPBA), a markedly different UV/vis absorption spectrum would be expected for both systems if the peracid unit was coordinated to the nickel in **2** and this is not the case. Moreover, formation of a nickel(III)-oxyl species by heterolytic O-O bond cleavage is in agreement with the much higher reactivity of the present system in comparison with previously reported well defined Ni/*m*CPBA species.[16, 29]
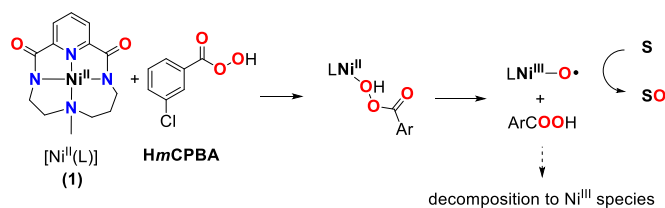
Scheme 3. Schematic representation of the nickel species formed upon reaction of **1** with H*m*CPBA.

Conclusions

The nickel(II) complex of the bis-amidate macrocyclic ligand (L) reacts with H*m*CPBA at low temperatures to form compound **2**, which has been spectroscopically trapped. This species is kinetically competent to perform the oxidation of different substrates such as olefins, sulfides and C-H bonds. Remarkably, its activity is much higher than that previously established for well-defined Ni-oxygen systems, which suggests that an alternative mechanism is occurring for the present system. Combination of experimental and theoretical results suggest that a heterolytic O-O bond cleavage in a Ni-H*m*CPBA adduct occurs, which gives rise to the formation of high-valent nickel-oxygen species which is best formulated as a Ni^{III}-oxyl. This work suggests that the use of a dianionic ligand may lead to alternative reaction pathways compared to previous systems, thus favouring the formation of high-valent nickel species that behave as strong oxidants. In this line, research in our group is aimed at ligand tuning and the use of alternative oxidants to further increase the reactivity of the nickel compound.

Experimental Section

Materials and methods

Reagents and solvents used were commercially available and purchased from Panreac, Scharlau and Aldrich. Preparation and handling of air-sensitive materials were carried out in a N_2 drybox (MBraun ULK 1000) with O_2 and H_2O concentrations < 1 ppm. Commercially available 70% *meta*-chloro-perbenzoic acid was purified prior to its use following A reported procedure.[42] The deuterated substrate d_4-9,10-dihydroanthracene was prepared from 9,10-dihydroanthracene following previously reported procedures.[43]

Elemental analyses of C, H and N were performed with a Perkin Elmer EA2400 series II elemental analyzer. Mass spectra were performed by electrospray ionization in a high-resolution mass spectrometer Bruker micrOTOF QII (Q-TOF) with a quadrupole analyzer with positive and negative ionization modes. ^{1}H-NMR, ^{13}C-NMR, COSY and HSQC spectra were performed in a Bruker Ultrashield Avance III400 and Ultrashield DPX300 spectrometers. UV/Vis absorption spectra were performed by a diode array spectrophotometer Agilent Cary 60 and low temperature control was maintained with a cryostat from Unisoku Scientific Instruments. X-ray analyses were carried out on BRUKER SMART APEX CCD diffractometer using graphite-monochromated Mo Kα radiation (λ = 0.71073 Å) from an X-ray tube. GC analyses were carried out on an Agilent 7820A gas chromatograph (HP5 column, 30m) with a flame ionization detector. GC-MS spectral analyses were performed on an Agilent 7890A gas chromatograph interfaced with an Agilent 5975c mass spectrometer with Triple-axis detector. CO_2 identification was carried out with an Agilent 7820A GC system equipped with three columns, washed molecular sieves 5Å, 2 m × 1/8 inch outside diameter (OD), Mesh 60/80 SS and Porapak Q, 4 m × 1/8 inch OD, Mesh 80/100 SS, and a thermal conductivity detector. Raman spectra were recorded in 5 mm diameter NMR tubes at 77 K in a liquid nitrogen filled quartz dewar. Spectra were collected in 180° back-scattering mode with excitation at 457 nm (Cobolt Lasers, 50 mW) with a dichroic mirror (Semrock) at 45° and a 150 mm focal length, 25 mm diameter planoconvex lens to focus the excitation beam and collect and collimate Raman scattering, which was passed through the dichroic and a long pass cut off filter (Semrock) before being focused at the entrance slits of a Shamrock 303i spectrograph with a 1200 l/mm grating blazed at 500 nm and a iDUS-420-BRDD CCD detector (Andor Technology). Spectral calibration was carried out using a 1:1 v/v mixture of acetonitrile and toluene. Spectra were processed using Andor Solis and Spectrum 10 (Perkin Elmer). Cyclic voltammetry was performed using a potentiostat from CHInstruments with a three electrode cell. The working electrode is a glassy carbon disk from BAS (0.07 cm^2), the reference electrode is a

saturated KCl calomel (SCE) and the auxiliary electrode is platinum wire. Voltammetry was carried out with nBu$_4$NPF$_6$ (TBAP) as supporting electrolyte (0.1 M ionic strength). EPR spectra were recorded with an ESP 300 X-Band EPR spectrometer from Bruker with a TE011 super high Q microwave resonator. Samples were cooled to 77 K with a liquid nitrogen Dewar. Spin quantifications were calculated on the basis of double integrals of the recorded spectra in comparison to a measured Cu^{II}-standard with a given concentration. Sample tubes were filled higher than the cavity dimension to guarantee an equally filled cavity for all measured samples. Spin quantifications were additionally corrected for volume errors resulting in slight differences in tube diameter.

A XX mM sample of **2** (prepared by reaction of **1** with x equiv HmCPBA in CH_3CN at xx ºC) was loaded into a 2mm holder with Kapton tape windows and stored at liquid nitrogen temperatures until run. Data was collected at the SOLEIL synchrotron SAMBA beamline equipped with a Si(220) double crystal monochromator and a liquid helium cryostat (20 K). X-ray absorption (XAS) was detected in fluorescence mode using a Canberra 35-element Ge detector and a Z-1 filter. An internal energy calibration was performed using the first inflection point of the X-ray absorption near edge structure (XANES) spectrum of nickel foil (E$_{cal}$ of 8331.6 eV). Data reduction and normalization was performed with the Athena software package using the AUTOBK algorithm. In order to extract intensities and energy positions the XANES pre-edge and edge were fit with pseudo-Voigt functions and the edge jump was modeled via a cumulative Gaussian-Lorentzian sum function. EXAFS were extracted using a R$_{bkg}$ of 1.05 Å and a spline between a k of 1 and 13.7 Å^{-1}. The Artemis software program using the IFEFFIT engine and FEFF6 code was used for EXAFS analysis.[44-46] The k^3-weighted data was fit in r-space over a k range of 2 - 12 Å^{-1}, with an S$_0$ value of 0.9 and a Kaiser-Bessel window (dk 2). The spectra were not phase corrected and a global ΔE_0 was employed, with the initial E$_0$ set to the inflection point of the rising edge at 8344.2 eV. Single scatter paths for Ni-N with initial R$_{eff}$ of 1.8 and 2.0 Å as well as multiple scattering from pyridine (initial R$_{eff}$ 1.8 Å) were fit in terms of ΔR_{eff} and σ^2 as previously described.[47-49] To assess the goodness of fit from different models both the R$_{factor}$ (%R) and the reduced χ^2 (χ^2_v) were minimized. While the R$_{factor}$ is generally expected to decrease with the number of adjustable parameters, χ^2_v may eventually increase, indicating the model is over-fitting the data.[50]

Synthesis of the Ni^{II}(CH$_3$CN)$_3$(OTf)$_2$. In a 100 mL Schlenk flask, NiCl$_2$ (2.36g, 0.018 mmol) was mixed with 50 mL of dry acetonitrile. Then, Me$_3$SiOTf (7.1 mL, 0.039 mmol) was added to the solution under a N_2 atmosphere. The skin coloured solution suspension was stirred vigorously at room temperature for 3 weeks while the colour darkened to deep blue. After that, the mixture was filtered to remove the starting material and the organic layer was then evaporated under reduced pressure, and a purple precipitate was formed. The solid was collected, dissolved in acetonitrile (5 mL) and slow diethyl ether diffusion at room temperature over the resulting solution afforded a purple solid, which after being dried under vacuum yielded Ni^{II}(CH$_3$CN)$_3$(OTf)$_2$ as a pale purple solid (5.43 g, 0.011 mmol, 63%). Anal. Calcd for C$_8$H$_9$F$_6$N$_3$NiO$_6$S$_2$: C, 20.02; N, 8.75; H, 1.89 %. Found: C, 19.76; N, 8.63; H, 1.97 %.

Synthesis of [Ni^{II}(L)] (1). In the glove box, a solution of Ni^{II}(CH$_3$CN)$_3$(OTf)$_2$ (32.09 mg, 0.057 mmol) in anhydrous acetonitrile (0.5 mL) was added dropwise to a vigorously stirred suspension of H$_2$L (15.10 mg, 0.057 mmol) in anhydrous acetonitrile (0.5 mL). After a few seconds the solution became colourless. Addition of 2 equiv NaH (2.71 mg, 0.11 mmol) caused a further colour change to orange. After stirring for 3 h, solvent was removed and the resulting residue dissolved in methanol, filtered through Celite® and concentrated. Slow diethyl ether diffusion over the resulting solution afforded, in a few days, **1** as orange crystals (20.07 mg, 0.041 mmol, 72%). ESI-MS (m/z): 341.05 [M+Na]$^+$ (100), 659.12 [2M+Na]$^+$ (40). ^{1}H-NMR (CD$_3$CN, 400 MHz, 298K) δ, ppm: 7.95 (t, J = 7.6 Hz, 1H, **H$_a$**), 7.43 (dd, J = 7.6 Hz, 1H, **H$_b$**), 7.36 (dd, J = 7.6Hz, 1H, **H$_c$**), 3.43-3.35 (m, 1H, **H$_d$**), 3.33-3.20 (m, 3H, **H$_{e/f/g}$**), 2.94-2.87 (m, 1H, **H$_h$**), 2.82-2.74 (m, 1H, **H$_i$**), 2.73-2.71 (m, 1H, **H$_j$**), 2.69 (s, 3H, **CH$_3$**), 2.50-2.45 (m, 1H, **H$_k$**), 1.81-173 (m, 2H, **H$_{l/m}$**). ^{13}C-NMR (CD$_3$CN, 100 MHz, 298K) δ, ppm: 169.39 (C$_{12}$

or C_{13}), 166.14 (C_{12} or C_{13}), 153.54 (C_{10} or C_{11}), 152.53 (C_{10} or C_{11}), 141.27 (C_1), 121.72 (C_2), 121.60 (C_3), 65.38 (C_4), 58.28 (C_5), 41.54 (C_6), 41.23 (C_7), 40.90 (C_8), 26.21 (C_9). Anal. Calcd. for $C_{13}H_{16}N_4NiO_2 \cdot NaOTf$: C, 34.24; H, 3.28; N, 11.61 Found: C, 33.98; H, 3.08; N, 11.23. CV (CH_3CN vs SCE): $E_{1/2}$ = 0.96 V.

Generation of 2. In a typical experiment, 2.5 mL of a 0.24 mM solution of **1** in acetonitrile were placed in a 1 cm path-length cuvette (0.6 μmols of **1**). The quartz cell was placed in the Unisoku cryostat of the UV-Vis absorption spectrophotometer and cooled down to 243 K. After reaching thermal equilibrium an UV/Vis absorption spectrum of the starting complex was recorded. Then, 105 μL of a 17 mM solution of HmCPBA in acetonitrile were added (3 equiv). The formation of a band at λ_{max} = 420 nm (ε = 7000 $M^{-1}cm^{-1}$) and a shoulder at λ_{max} = 580 nm (ε = 800 $M^{-1}cm^{-1}$) was observed. **2** was fully formed within 100 s.

Analysis of the reaction of 2 with substrates. Once **2** was fully formed, 150 μL of a solution containing the corresponding equivalents of the desired substrate were added in the cuvette. The decay of the band at λ = 420 nm was monitored and after complete decay the solution was quenched by adding an excess of $NaHSO_3$ (0.1 mL of a commercially available 40 % aqueous solution). Biphenyl was added as internal standard and the nickel complex was removed by passing the solution through a short plug of silica. The products were then eluted with ethyl acetate and analysed by GC-FID. The organic products were identified by comparison with authentic compounds.

Catalytic experiments at room temperature with HmCPBA. In a typical reaction, 0.5 mL of a 0.58 M solution of HmCPBA (290 μmol) in acetonitrile were delivered by syringe pump over 30 min at 25 ºC to a vigorously stirred acetonitrile solution (2.5 mL) containing the nickel catalyst (2.0 μmol) and the substrate (1900 μmol). The final concentrations of reagents were 0.7 mM nickel catalyst, 97 mM HmCPBA, and 0.62 M substrate. After syringe pump addition, the resulting solution was stirred for another 30 min. For the oxidation of cyclohexane, biphenyl was added as internal standard and the nickel complex was removed by passing the solution through a short path of silica. The products were then eluted with ethyl acetate and then analysed by GC-FID. The organic products were identified by comparison with authentic compounds.

Computational details

All DFT calculations were carried out with the Gaussian09 set of programs.[51] X-ray diffraction structure of [Ni^{II}(L)] (**1**) has been chosen as starting point for geometry optimizations, using the B3LYP exchange-correlation functional[52, 53] and the TZVP basis set.[54] Nickel species were considered in all possible spin states without symmetry constraints. The CH_3CN solvation and effects were included in geometry optimizations through the SMD polarizable continuum model.[55] Dispersion effects were introduced through single point calculations with the Grimme's D_3 correction with Becke-Johnson damping.[56] The connection between transition states and minimums was verified by intrinsic reaction coordinate (IRC) calculations.

Hirshfeld's spin densities and charges, Mayer bond order index[57, 58] and spin natural orbitals (SNO) were computed to rationalize the electronic structure of intermediate **2**. A Bader's AIM analysis (Atom-In-Molecule)[59-61] was also conducted on **2** to elucidate the nature of the Ni-O bond.

Analytical frequency calculations were performed to evaluate the thermal corrections and entropic effects at 243.15 K, as well as to characterize the located stationary points in condensed phase. Raman spectra intensities of intermediate **2** were simulated at 77 K and with a laser excitation of 457 nm using the GaussSum 3.0 software.[62]

Final Gibbs energies (G) were evaluated with the following equation:

$$G = E_{TZVP}(SMD + D_3) + G_{corr.} \quad (1)$$

where $E_{TZVP}(SMD+D_3)$ is obtained through single point calculations with the TZVP basis set on equilibrium geometries, including the solvation and dispersion effects, and $G_{corr.}$ is the thermal correction obtained from a thermo-statistical analysis at the B3LYP/SMD level.

The pK_a values were computed according to:

$$pK_a = \frac{\Delta G^o}{RT \ln(10)} \quad (2)$$

where R is the universal gas constant and T is the temperature.[63] The standard dissociation free energy change (ΔG^o) between an acid (AH) and its conjugate base (A$^-$) in solvent phase may be calculated using the following equations:

$$\Delta G^o = G(A^-_{sol}) + G(H^+_{sol}) - G(AH_{sol}) + \Delta G^* \quad (3)$$

$$G(H^+_{aq}) = G(H^+_{gas}) + \Delta G^{H+}_{solv} \quad (4)$$

where $G(AH_{sol})$ and $G(A^-_{sol})$ are the standard free energies of the acid and its conjugate base, respectively. The $G(H^+_{sol})$ is the free energy of the proton in acetonitrile, obtained from the solvation free energy of a proton in acetonitrile ($\Delta G^{H+}_{solv} = -260.2 \text{ kcal} \cdot \text{mol}^{-1}$)[55] and its gas-phase free energy ($G(H^+_{gas}) = -6.3 \text{ kcal} \cdot \text{mol}^{-1}$).[56] ΔG^* is the standard state thermodynamic correction associated with the conversion from a standard-state of 1 M in the aqueous phase and 1 atm in gas phase, to 1 M in both phases. Its value is 1.54 kcal•mol^{-1} at 243.15 K.

Acknowledgements

Notes and references

[1] S. B. Mulrooney, R. P. Hausinger, *FEMS Microbiol. Rev.* **2003**, *27*, 239-261.
[2] H. Ogata, W. Lubitz, Y. Higuchi, *Dalton Trans.* **2009**, 7577-7587.
[3] H. Dobbek, V. Svetlitchnyi, L. Gremer, R. Huber, O. Meyer, *Science* **2001**, *293*, 1281-1285.
[4] T. I. Doukov, T. M. Iverson, J. Seravalli, S. W. Ragsdale, C. L. Drennan, *Science* **2002**, *298*, 567-572.
[5] H.-D. Youn, E.-J. Kim, J.-H. Roe, Y. C. Hah, S.-O. Kang, *Biochem. J.* **1996**, *318*, 889-896.
[6] M. Sankaralingnam, M. Balamuruguan, M. Palaniandavar, V. P, C. H. Suresh, *Chem. Eur. J.* **2014**, *20*, 11346-11361.
[7] X. Solans-Monfort, J. L. G. Fierro, L. Hermosilla, C. Sieiro, M. Sodupe, R. Mas-Ballesté, *Dalton Trans.* **2011**, *40*, 6868-6876.
[8] S. Z. Tasker, E. A. Standley, T. F. Jamison, *Nature* **2014**, *509*, 299-309.
[9] Y. Aihara, N. Chatani, *J. Am. Chem. Soc.* **2014**, *136*, 898-901.
[10] T. Nagataki, K. Ishii, Y. Tachi, S. Itoh, *Dalton Trans.* **2007**, 1120-1128.
[11] T. Nagataki, Y. Tachi, S. Itoh, *Chem. Commun.* **2006**, 4016-4018.
[12] M. Balamurugan, R. Mayimurugan, E. Suresh, M. Palaniandavar, *Dalton Trans.* **2011**, *40*, 9413-9424.
[13] D. Schröder, H. Schwarz, *Angew. Chem. Int. Ed.* **1995**, *34*, 1973-1995.
[14] Y. Shiota, K. Yoshizawa, *J. Am. Chem. Soc.* **2000**, *122*, 12317-12326.

[15]   A. Company, J. Lloret-Fillol, M. Costas, in *Comprehensive Inorganic Chemistry II, Vol. 3* (Eds.: J. Reedijk, K. Poeppelmeier), Elsevier, Oxford, **2013**.

[16]   F. F. Pfaff, F. Heims, S. Kundu, S. Mebs, K. Ray, *Chem. Commun.* **2012**, *48*, 3730-3732.

[17]   S. Hikichi, K. Hanaue, T. Fujimura, H. Okuda, J. Nakazawa, Y. Ohzu, C. Kobayashi, M. Akita, *Dalton Trans.* **2013**, *42*, 3346-3356.

[18]   P. Pirovano, E. R. Farquhar, M. Swart, A. J. Fitzpatrick, G. G. Morgan, A. R. McDonald, *Chem. Eur. J.* **2015**.

[19]   A. K. Patra, R. Mukherjee, *Inorg. Chem.* **1999**, *38*, 1388-1393.

[20]   P. J. Donoghue, J. Tehranchi, C. J. Cramer, R. Sarangi, E. I. Solomon, W. B. Tolman, *J. Am. Chem. Soc.* **2011**, *133*, 17602-17605.

[21]   D. Huang, R. H. Holm, *J. Am. Chem. Soc.* **2010**, *132*, 4693-4701.

[22]   S. K. Sharma, S. Upreti, R. Gupta, *Eur. J. Inorg. Chem.* **2007**, 3247-3259.

[23]   D. H. Lee, J. Y. Lee, J. Y. Ryu, Y. Kim, C. Kim, I.-M. Lee, *Bull. Korean Chem. Soc.* **2006**, *27*, 1031-1037.

[24]   Y. Goto, T. Matsui, S. Ozaki, Y. Watanabe, S. Fukuzumi, *J. Am. Chem. Soc.* **1999**, *121*, 9497-9502.

[25]   F. A. Carey, R. Giuliano, *Orgnaic Chemistry*, 9th ed., McGraw-Hill, **2013**.

[26]   V. W. Manner, T. F. Markle, J. H. Freudenthal, J. P. Roth, J. M. Mayer, *Chem. Commun.* **2008**, 256-258.

[27]   C. V. Sastri, J. Lee, K. Oh, Y. J. Lee, J. Lee, T. A. Jackson, K. Ray, H. Hirao, W. Shin, J. A. Halfen, J. Kim, L. Que, S. Shaik, W. Nam, *Proc. Natl. Acad. Sci. USA* **2007**, *104*, 19181-19186.

[28]   J. M. Mayer, *Acc. Chem. Res.* **1998**, *31*, 441-450.

[29]   J. Nakazawa, S. Terada, M. Yamada, S. Hikichi, *J. Am. Chem. Soc.* **2013**, *135*, 6010-6013.

[30]   M. Costas, K. Chen, L. Que, *Coord. Chem. Rev.* **2000**, *200*, 517-544.

[31]   Y. H. Huang, J. B. Park, M. W. W. Adams, M. K. Johnson, *Inorg. Chem.* **1993**, *32*, 375-376.

[32]   C.-M. Lee, C.-H. Chen, F.-X. Liao, C.-H. Hu, G.-H. Lee, *J. Am. Chem. Soc.* **2010**, *132*, 9256-9258.

[33]   N. Yang, M. Reiher, M. Wang, J. Harmer, E. C. Duin, *J. Am. Chem. Soc.* **2007**, *129*, 11028-11029.

[34]   M. Dey, J. Telser, R. C. Kunz, N. S. Lees, S. W. Ragsdale, B. M. Hoffman, *J. Am. Chem. Soc.* **2007**, *129*, 11030-11032.

[35]   G. J. Colpas, M. J. Maroney, C. Bagyinka, M. Kumar, W. S. Willis, S. L. Suib, N. Baidya, P. K. Mascharak, *Inorganic Chemistry* **1991**, *30*, 920-928.

[36]   L. R. Furenlid, M. W. Renner, E. Fujita, *Physica B* **1995**, *208*, 739-742.

[37]   W. E. Ogrady, K. I. Pandya, K. E. Swider, D. A. Corrigan, *Journal of the Electrochemical Society* **1996**, *143*, 1613-1616.

[38]   M. Risch, K. Klingan, J. Heidkamp, D. Ehrenberg, P. Chernev, I. Zaharieva, H. Dau, *Chemical Communications* **2011**, *47*, 11912-11914.

[39]   J. Bernadou, B. Meunier, *Chem. Commun.* **1998**, 2167-2173.

[40]   D. Moonshiram, I. Alperovich, J. J. Concepcion, T. J. Meyer, Y. Pushkar, *Proc. Natl. Acad. Sci. USA* **2013**, *110*, 3765-3770.

[41]   B. Lassalle-Kaiser, C. Hureau, D. A. Pantazis, Y. Pushkar, R. Guillot, V. K. Yachandra, J. Yano, F. Neese, E. Anxolabéhère-Mallart, *Energy Environ. Sci.* **2010**, *3*, 924-938.

[42]   V. K. Aggarwal, Z. Gültekin, R. S. Grainger, H. Adams, P. L. Spargo, *J. Chem. Soc., Perkin Trans. 1* **1998**, 27714-22782.

[43]   C. R. Goldsmith, R. T. Jonas, T. D. P. Stack, *J. Am. Chem. Soc.* **2002**, *124*, 93-96.

[44]   M. Newville, *Journal of Synchrotron Radiation* **2001**, *8*, 96-100.

[45]   B. Ravel, M. Newville, *Journal of Synchrotron Radiation* **2005**, *12*, 537-541.

[46]   J. J. Rehr, R. C. Albers, *Reviews of Modern Physics* **2000**, *72*, 621-654.

[47]   K. Banaszak, V. Martin-Diaconescu, M. Bellucci, B. Zambelli, W. Rypniewski, M. J. Maroney, S. Ciurli, *Biochemical Journal* **2012**, *441*, 1017-1026.

[48]   V. Martin-Diaconescu, M. Bellucci, F. Musiani, S. Ciurli, M. J. Maroney, *Journal of Biological Inorganic Chemistry* **2012**, *17*, 353-361.

[49]   B. Zambelli, A. Berardi, V. Martin-Diaconescu, L. Mazzei, F. Musiani, M. J. Maroney, S. Ciurli, *Journal of Biological Inorganic Chemistry* **2014**, *19*, 319-334.

[50]   R. W. Herbst, I. Perovic, V. Martin-Diaconescu, K. O'Brien, P. T. Chivers, S. S. Pochapsky, T. C. Pochapsky, M. J. Maroney, *Journal of the American Chemical Society* **2010**, *132*, 10338-10351.

[51]   M. J. Frisch, G. W. Trucks, H. B. Schlegel, G. E. Scuseria, M. A. Robb, J. R. Cheeseman, G. Scalmani, V. Barone, B. Mennucci, G. A. Petersson, H. Nakatsuji, M. Caricato, X. Li, H. P. Hratchian, A. F. Izmaylov, J. Bloino, G. Zheng, J. L. Sonnenberg, M. Hada, M. Ehara, K. Toyota, R. Fukuda, J. Hasegawa, M. Ishida, T. Nakajima, Y. Honda, O. Kitao, H. Nakai, T. Vreven, J. A. Montgomery, Jr., J. E. Peralta, F. Ogliaro, M. Bearpark, J. J. Heyd, E. Brothers, K. N. Kudin, V. N. Staroverov, R. Kobayashi, J. Normand, K. Raghavachari, A. Rendell, J. C. Burant, S. S. Iyengar, J. Tomasi, M. Cossi, N. Rega, M. J. Millam, M. Klene, J. E. Knox, J. B. Cross, V. Bakken, C. Adamo, J. Jaramillo, R. Gomperts, R. E. Stratmann, O. Yazyev, A. J. Austin, R. Cammi, C. Pomelli, J. W. Ochterski, R. L. Martin, K. Morokuma, V. G. Zakrzewski, G. A. Voth, P. Salvador, J. J. Dannenberg, S. Dapprich, A. D. Daniels, Ö. Farkas, J. B. Foresman, J. V. Ortiz, J. Cioslowski, D. J. Fox, Gaussian, Inc., Wallingford CT, **2009**.

[52]   A. D. Becke, *J. Chem. Phys.* **1993**, *98*, 1372-1377.

[53]   A. D. Becke, *J. Chem. Phys.* **1993**, *98*, 5648-5652.

[54]   A. Schaefer, C. Huber, R. Ahlrichs, *J. Chem. Phys.* **1994**, *100*, 5829-5835.

[55]   A. V. Marenich, C. J. Cramer, D. G. Truhlar, *J. Phys. Chem. B* **2009**, *113*, 6378-6396.

[56]   S. Grimme, S. Ehrlich, L. Goerigk, **2011**, *32*, 1456-1465.

[57]   I. Mayer, *Chem. Phys. Lett.* **1983**, *97*, 270-274.

[58]   I. Mayer, *Int. J. Quantum Chem.* **1984**, *26*, 151-154.

[59]   R. F. W. Bader, *J. Phys. Chem. A* **1998**, *102*, 7314-7323.

[60]   R. F. W. Bader, *Atoms in Molecules: A Quantum Theory*, Oxford University Press, Oxford, **1990**.

[61]   F. Bieger-Kim, AIM Version 1.0. University of Applied Science, Bielefeld, Germany, **2000**.

[62]   N. M. O'Boyle, A. L. Tenderholt, K. M. Langner, *J. Comput. Chem.* **2008**, *29*, 839-845.

[63]   C. P. Kelly, C. J. Cramer, D. G. Truhlar, *J. Phys. Chem. B* **2006**, *110*, 2493-2499.